Journal of Materials Science: Materials in Medicine (2019) 30:43
https://doi.org/10.1007/s10856-019-6241-y

ENGINEERING AND NANO-ENGINEERING APPROACHES FOR MEDICAL DEVICES

Original Research

Osteoblast adhesion and response mediated by terminal –SH group charge surface of SiOxCy nanowires

Benedetta Ghezzi[1,2] · Paola Lagonegro[3,4] · Roberta Pece[1,2,5] · Ludovica Parisi[1,2] · Massimiliano Bianchi[2] · Roberta Tatti[6] · Roberto Verucchi[6] · Giovanni Attolini[4] · Martina Quaretti[4] · Guido M. Macaluso[1,2,3]

Received: 17 October 2018 / Accepted: 18 February 2019 / Published online: 30 March 2019

Abstract

Robust cell adhesion is known to be necessary to promote cell colonization of biomaterials and differentiation of progenitors. In this paper, we propose the functionalization of Silicon Oxycarbide (SiO_xC_y) nanowires (NWs) with 3-mercaptopropyltrimethoxysilane (MPTMS), a molecule containing a terminal –SH group. The aim of this functionalization was to develop a surface capable to adsorb proteins and promote cell adhesion, proliferation and a better deposition of extracellular matrix. This functionalization can be used to anchor other structures such as nanoparticles, proteins or aptamers. It was observed that surface functionalization markedly affected the pattern of protein adsorption, as well as the in vitro proliferation of murine osteoblastic cells MC3T3-E1, which was increased on functionalized nanowires (MPTMS-NWs) compared to bare NWs (control) ($p < 0.0001$) after 48 h. The cells showed a better adhesion on MPTMS-NWs than on bare NWs, as confirmed by immunofluorescence studies on the cytoskeleton, which showed a more homogeneous vinculin distribution. Gene expression analysis showed higher expression levels for alkaline phosphatase and collagen I, putative markers of the osteoblast initial differentiation stage. These results suggest that functionalization of SiO_xC_y nanowires with MPTMS enhances cell growth and the expression of an osteoblastic phenotype, providing a promising strategy to improve the biocompatibility of SiO_xC_y nanowires for biomedical applications.

Graphical Abstract

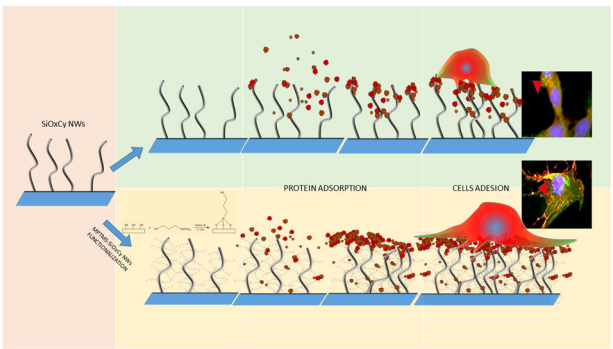

These authors contributed equally: Benedetta Ghezzi, Paola Lagonegro

✉ Paola Lagonegro
lagonegro@ismac.cnr.it

[1] Centro Universitario di Odontoiatria, University of Parma, Via Gramsci 14, 43126 Parma, Italy

[2] Dipartimento di Medicina e Chirurgia, University of Parma, Via Gramsci 14, 43126 Parma, Italy

[3] ISMAC-CNR, Institute for macromolecular studies, Via Corti, 12, 20133 Milano, Italy

[4] IMEM-CNR, Institute of Materials for Electronics and Magnetism, Parco Area delle Scienze, 37/A, 43124 Parma, Italy

[5] School of Medicine, University of Genoa, DIMES, L.go R. Benzi 10, Genoa 16131, Italy

[6] IMEM-CNR, Institute of Materials for Electronics and Magnetism, Trento unit, Via alla Cascata, 56/C, 38123 Trento, Italy

1 Introduction

Implant scaffold materials for tissue regeneration should provide the organism with chemical, geometric and physical cues that are compatible with cell differentiation pathways [1, 2]. This approach may act as surrogate niches to support cell activity and guide cell commitment and maturation to a desired phenotype that is then able to generate pristine tissue [3]. A vast array of materials have been proposed, ranging from grafted tissues [4], tissue derivatives [5, 6], or synthetic materials [2, 7, 8]. Both the physico-chemical features of scaffolds and their structure have been proven to affect scaffold behavior and, particularly, the micro- and nanostructure have been shown to be able to control cell responses [9, 10]. The emergence of nanotechnologies may now open up numerous possibilities to apply nano-patterned features to biomaterials to modulate their surfaces, so that they comply with the nanoscale features of the natural cells microenvironment [11]. Nanowires (NWs) appear as potential candidates for the design of biomimetic materials with defined nanoscale patterns to induce cell proliferation and differentiation. They are one dimensional structures, arranged in three-dimensional (3D) meshworks, which strikingly mimic the spatial organization of several extracellular environments, such as the dental alveolar matrix or collagen I fibers [12]. Therefore, it is possible to hypothesize that NWs could be used to create implantable scaffolds to promote tissue regeneration [13]. Among candidate raw materials NWs can be made of silicon-derivatives, which display interesting features for clinical applications. Silicon oxycarbide (SiO_xC_y) possesses high elastic modulus, bending strength and hardness, as well as chemical durability and stability [14]. Moreover, SiO_xC_y has been shown to promote platelet activation, thus prompting rapid clot formation, which is a necessary feature for wound healing [15]. However, when compared to the natural extracellular matrix, bare NWs lack the capability to establish specific interactions with molecular components that may enhance cell adhesion or function. Fortunately, SiO_xC_y can be easily engineered through functionalization and decoration with macro-molecules [16, 17], which make NWs a suitable platform for several experimental biomimetic approaches.

Herein, we show that nanowires can be employed for efficiently amplifying the effect of surface charge on cell adhesion. Therefore, this study will help us understand the regulation of biomaterials on cell adhesion and may allow for the development of new biomedical materials with tailored cell adhesion for tissue implantation and regeneration.

NWs were functionalized with 3-mercaptopropyltrimethoxysilane (MPTMS), a molecule that is capable to interact with silicon oxide through its silane group, and that can provide free thiol groups to covalently bind and retain proteins from plasma through the formation of solid disulfide bridges. Indeed, it is known that cells cultured in contact with–SH-modified surfaces promoted osteogenesis in vitro [18].

In this framework, the hypothesis underlying our work is the possibility to ameliorate protein adsorption, cell adhesion and osteoblast differentiation on NWs by modifying their surface chemistry and charge.

2 Materials and methods

We developed and characterized –SH modified SiO_xC_y nanowire-surfaces; the presence of MPTMS was first evaluated through X-ray Photoelectron Spectroscopy and changes in the surface electronegativity observed with Z-potential analysis. After surface characterization, in vitro experiments were performed to observe serum protein adsorption. Osteoblast response to the materials was studied through viability assays, cell morphology observation and gene expression quantification; adhesion was analyzed with immunofluorescence of cell for focal adhesion.

2.1 MPTMS-NWs synthesis

Amorphous SiO_xC_y NWs were grown on Si substrates by an established Chemical Vapor Deposition (CVD) process, lowering the growth temperature to 1070 °C [19]. In this process, carbon monoxide acts as a dopant precursor, so that carbon-doped under-stoichiometric silicon dioxide NWs are obtained [20]. The typical SiO_xC_y NW length was several tens of μm whereas the average diameter was approximately 100 nm. After their synthesis, the NWs were analyzed by Field-Emission Scanning Electron Microscopy (SEM) in a Zeiss Auriga Compact system (Zeiss, Oberkochen, Germany), to select samples with a homogeneous coverage of the substrate with a dense NW network on the order of 10 NWs/μm^2.

2.2 MPTMS-NWs functionalization

The Si substrates covered with SiO_xC_y NWs were soaked in 10 ml of toluene. Then, 15 μl of 3 mM 3-mercaptopropyltrimethoxysilane (MPTMS, 95% pure, Sigma-Aldrich, Milan, Italy) solution was added and the mixture incubated at room temperature under N_2 atmosphere for 24 h (Fig. 1). After that, the samples were rinsed in toluene and dried in vacuum.

2.3 X-ray photoelectron Spectroscopy

NWs functionalization was checked ex situ by X-ray Photoelectron spectroscopy (XPS), using as the X-ray photon source Mg-Kα emission at 1253.6 eV. Photoelectrons were

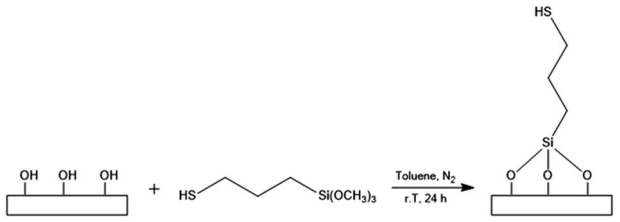

Fig. 1 Diagram showing the functionalization strategy followed in the present work. 3-mercaptopropyltrimethoxysilane was anchored to the NW by binding to –OH groups on the NW surface, so that additional free –thiol groups were supplied, for protein binding

analyzed by a VSW HA100 hemispherical analyzer, with a total energy resolution of 0.86 eV. The core level positions, indicated by their Binding Energy (BE), were calibrated using as reference the Au 4 f 7/2 peak at 84.00 eV. The lineshape of all core levels (C1s, O1s, Si2p and S2p) were analyzed using a Voight function, with a Lorentzian-Gaussian fixed ratio of 0.3, following a Shirley background subtraction. The uncertainty related to the energy peak position was ± 0.05 eV, while the precision for full width at half-maximum (FWHM) and for area evaluation was less than ± 5% and ± 2.5%, respectively.

2.4 Z-potential characterization

To study the differences in surfaces electronegativity, a Z-Potential analysis was performed. NWs were detached from the substrate by ultrasonication using a Misonix, Ultrasonic Liquid Processor S-400 (New Highway, Farmingdale, NY 11735, USA). The NWs were then dispersed in Phosphate Buffer Saline solution (PBS, Thermo Fisher Scientific, Waltham, MA, USA), sonicated to obtain a homogeneous suspension and diluted in culturing medium. Finally, an aliquot was transferred to acrylic cuvettes and their Z-Potential was measured by a Zeta Potential Plus Analyzer (Brookhaven instruments Corporation, NY, USA).

2.5 Protein adsorption

To study serum proteins adsorption, samples were incubated in PBS (500 µl) supplemented with 2% Human Serum (HS, Sigma-Aldrich) for 1 h at room temperature (RT). The samples were then rinsed twice in PBS to remove any unstable adsorbed proteins and covered with 80 µl of Sample Buffer 1 × (Tris-HCl 62.5 mM pH 6.8, SDS 1.5%w/v, DTT 100 mM, with traces of Bromophenol Blue). Complete recovery of proteins was obtained by freezing, thawing, sonicating samples for 15 min, and boiling them for 10 min on a hot plate. Equal volumes of samples were then loaded on 12% polyacrylamide gel (Acrylamide/Bis-Acrylamide 30%, Sigma-Aldrich) and separated at 180 V for 1 h. The gels were then exposed to Coomassie solution (Coomassie Brilliant Blue, Bio-Rad, USA) for protein staining.

2.6 Cell culture

Osteoblastic MC3T3-E1 cells from mouse calvaria were obtained from the American Type Culture Collection (LGC Standards S.r.L., Sesto S. Giovanni, MI, Italy) and cultured in Alpha-MEM (□-MEM, Thermo Fisher Scientific, Carlsbad, CA; USA) with 10% Fetal Bovine Serum (FBS, Thermo Fisher Scientific) addition, 1% L-Glutammine (Thermo Fisher Scientific) and 1% Penicillin and Streptomycin (Penstrep, Sigma-Aldrich, St. Louis, MI, USA). For cell culture experiments, cells were seeded on Si substrates (size 0.5 cm × 0.5 cm) with NWs on top, at a final concentration of 2×10^4 cells/sample for viability assays, morphology observation and immunofluorescence and of 4×10^4 cells/sample for qRT-PCR analysis.

2.7 Cell viability assays

Cell viability was assayed 24 and 48 h after plating with chemiluminescence assay (Cell-Titer Glo, Promega, Milan, Italy), according to the manufacturer's indications. Briefly, culture medium was eliminated and a 50:50 solution of Cell-Titer Glo Lysis Buffer and complete αMEM was added to each sample. After shaking for 2 min, the solution was collected and luminescence was stabilized for 10 min in the dark. Subsequently, the luminescence was measured with a luminometer with double injectors (GLOMAX 20/20, Promega, Madison, WI, USA). Moreover, viable and dead cells were assessed 24 and 48 h after seeding via LIVE/DEAD assay, which involved the use of Calcein AM 4 µM (Sigma-Aldrich), specific for living cells and of Propidium Iodide 7.5 µM (Sigma-Aldrich), specific for dead cells. Briefly, the culture medium was replaced with a PBS solution containing Calcein AM and Propidium Iodide for 10 min at RT in the dark. Subsequently, the samples were washed in PBS and fixed for 20 min in paraformaldehyde 4% (PFA, Sigma-Aldrich) and observed through fluorescence microscopy (Axioscope, Zeiss).

2.8 Cell morphology

Scanning Electron Microscopy (SEM) was used in combination with orthogonal sample cutting using a Gallium Focused Ion Beam (FIB) source, to study cell morphology and their interactions with the underlying substrate. To perform the morphological assays 1×10^4 MC3T3-E1 cells were plated on samples as described above and SEM-FIB preparation was performed 48 h after seeding at RT. Briefly, culturing medium was removed and cells were rinsed in PBS (Sigma-Aldrich). Subsequently, cells were fixed in a

2.5% glutaraldehyde solution (Sigma-Aldrich) in Na-Cacodylate buffer (Sigma-Aldrich) for 30 min, washed in Na-Cacodylate buffer (Sigma-Aldrich) for 5 min, and dehydrated in ethanol at increasing concentrations (Sigma-Aldrich). Finally, samples were critical point dried with liquid carbon dioxide (CPD 030 Baltec, Wallruf, Germany) and sputtered with a thin layer of gold through a SCD 040 coating device (Balzer Union, Wallruf, Germany). Sample microphotographs were taken using a dual beam Zeiss Auriga Compact system equipped with a GEMINI Field-Effect SEM column and a Gallium Focused Ion Beam (FIB) source (Zeiss). SEM analysis was performed at 5 keV, while cross-sectional analysis with FIB was performed with a Gallium ion beam at 30 kV with a current of 10 pA.

2.9 Immunofluorescence

To observe the expression and distribution of focal adhesions, immunofluorescence staining was performed for focal adhesions, cytoskeleton and cell nuclei. After 48 h of culture, the culturing medium was removed, and cells were fixed in a 4% PFA solution for 10 min at RT. After two rinses in PBS, the cells were permeabilized with 0.1% v/v Triton X-100 (Sigma-Aldrich) for 5 min at RT and washed twice with PBS. To block antibody aspecific binding sites, 1% bovine serum albumin solution (BSA, Sigma-Aldrich) was added to the samples for 30 min at RT. The cells were then treated with a primary anti-Vinculin monoclonal antibody, clone 7F9 (1:100 dilution), (FAK100, Merck Millipore, Darmstadt, Germany), for 1 h at RT and subsequently washed twice in PBS. To reveal the primary anti-vinculin antibody, a secondary anti-mouse labeled with the Alexa-Fluor®488 chromophore (Thermo Fisher Scientific) (dilution 1:200) was co-incubated with TRITC-conjugated phalloidin (FAK100, Merck Millipore) (dilution 1:200) for actin staining. After three rinses with PBS, the nuclei were counterstained with DAPI solution 1:1000 (FAK100, Merck Millipore). The samples were observed and images taken with a stereomicroscope equipped for fluorescence (SMZ25, Nikon, Tokyo, Japan).

2.10 Real time PCR

After 96 h of culture, total RNA was extracted using TriZol (Thermo Fisher Scientific), according to the manufacturer's indications and then retro-transcribed to cDNA with a High capacity cDNA Reverse Transcription Kit (Thermo Fisher Scientific). TaqMan quantitative RT-PCR was performed using the following primer probe sets from Life Technologies (Foster City, CA, USA): Alkaline Phosphatase (Mm00475834_m1); Collagen 1a1 (Mm00801666_g1); Runx2 (Mm00501584_m1); Osteocalcin (for 5′-GCTGCG CTCTGTCTCTCTGA-3′ rev 5′-TGCTTGGACATGAAGG CTTTG-3′ probe 5′-FAM-AAGCCCAGCGGCC-NFQ-3′); mouse glyceraldehyde-3-phosphate dehydrogenase (GAPDH) was used as housekeeping gene (Mm99999915_g1). qRT-PCR was performed with a Real Time PCR machine (StepOne Plus, Life Technologies).

2.11 Statistical analysis

Data were analyzed using Prism 6 (GraphPad, La Jolla, CA). All values are reported as the mean ± standard deviation of three repeated experiments performed in triplicate. Differences between group means were evaluated with ANOVA statistical test and Tukey post test and differences were considered significant when $p < 0.05$.

3 Results

3.1 X-ray photoelectron spectroscopy analysis

Samples were first characterized by XPS analysis, performed on NWs before (Fig. 2, upper panel) and after functionalization (Fig. 2, lower panel). This technique allowed us to define the chemical composition of the samples in terms of surface atomic percentage and type of chemical bonds (C1s, O1s, Si2p and S2p). Specifically, the carbon total atomic percentage at the SiO_xC_y NW surface was 25.0%, which increased up to 31.1% following the functionalization with MPTMS, with the consequent decrement of the oxygen and silicon content (from 42.6 and 32.4% to 37.0 and 31.1%, respectively). Sulfur in the MPTMS-NWs amounted to 0.8% with respect to the total composition of the material, while no Sulfur was observed on bare NWs. Results of a detailed analysis for the C1s, O1s, Si2p and S2p peaks, in terms of binding energy (BE) and percentage calculated with respect the total core level area, are summarized in Table 1.

All core levels in the NW analysis were characterized by an energy shift of about 1.5 eV towards higher BE, with respect to the expected values [20], because of (not compensated) charging phenomena due to the insulating character of the material. The C1s core level NW spectrum (Fig. 2a) was characterized by four components associated to the Si–C bond (located at 285.27 eV), C–C/C–H (286.22 eV), oxycarbides such as SiOC, C–O (287.37 eV) and C=O groups (289.71 eV). The Si2p lineshape, in addition to the component related to the Si–C and SiOC bonds (103.69 and 104.74 eV), showed the typical contribution from SiOx at 105.69 eV (Fig. 2c). The corresponding peak of the latter in the O1s core level was located at 535.29 eV. The O1s lineshape deconvolution was moreover characterized by a further feature at 534.31 eV, that can be more generally related to SiOC, CO and C=O groups (showing similar

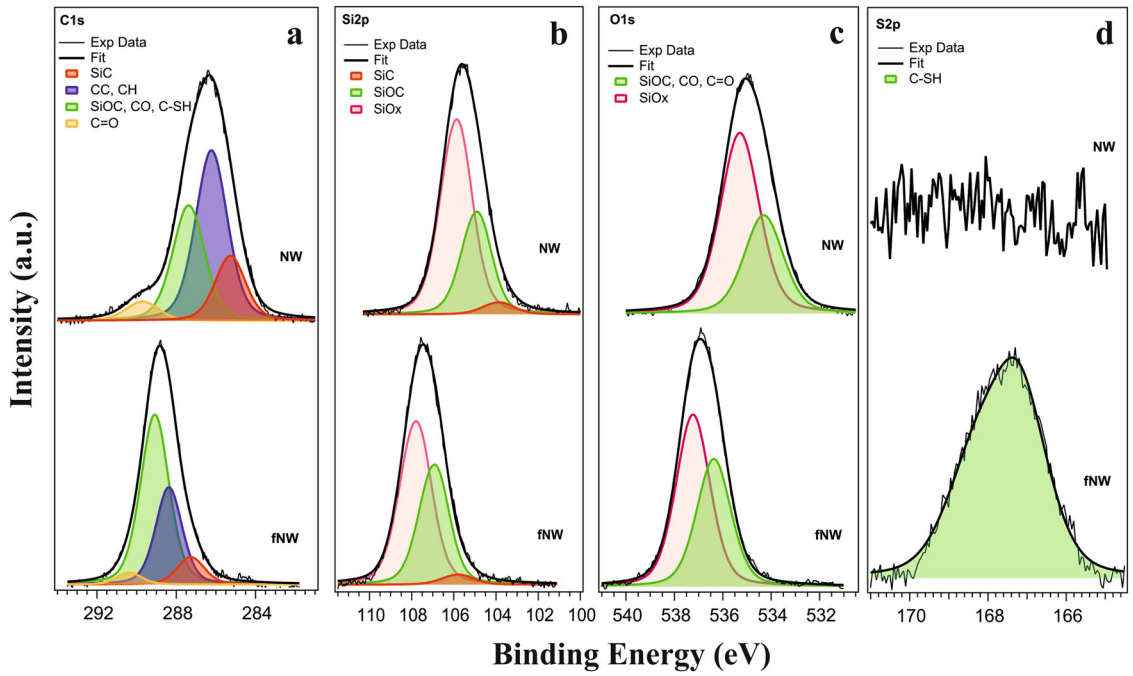

Fig. 2 XPS core level spectra (background subtracted): C1s **a**, O1s **b**, Si2p **c** and S2p **d** of bare NWs (upper panel) and MPTMS-NWs (lower panel)

Table 1 Features (binding energy and percentage of the total core level area) of the C1s, O1s, Si2p and S2p core levels of NWs and MPTMS-NWs samples

		NWs		MPTMS-NWs	
		BE [eV]	%	BE [eV]	%
C1s	SiC	285.27	16.8	287.27	8.9
	CC, CH	286.22	46.4	288.37	30.3
	SiOC, CO	287.37	31.4	289.08	57.3
	C=O	289.71	5.4	290.37	3.5
O1s	SiOC, CO, C=O	534.31	35.2	536.37	42.7
	SiOx	535.29	64.8	537.23	57.3
Si2p	SiC	103.69	3.9	105.62	3.5
	SiOC	104.74	31.8	106.75	39.4
	SiOx	105.69	64.3	107.62	57.1
S2p	C–SH	–	–	167.22	100

BEs). The analysis for all core levels was in agreement with studies previously reported in literature [19, 21].

In functionalized NWs a higher energy shift (~3.0 eV) was observed, suggesting that MPTMS further enhances the insulating character of the material. The core level lineshape of C1s, O1s and Si2p shows the same (shifted in BE) main components. Indeed, since MPTMS is composed of chemical species similar to NWs (in addition to Sulphur), this leads to a superposition of photoemission signals from the inorganic and the organic materials (see Fig. 2 and Table 1). As a matter of fact, it is worthy to note that the intensity of the Si–C, C–C and C=O components (287.27, 288.37 and 290.37 eV) in the C1s core level decreased, whereas an increase of the SiOC/C–O species (289.08 eV) occurred (Fig. 2a). This trend was in line with the expected molecular structure of MPTMS, with SiOC and C–S groups enhancing the intensity of the peak at 289.08 eV, being characterized by very similar Bes [21]. In the same way, the corresponding components in the Si2p (SiOC at 106.75 eV) and O1s (SiOC, C–O and C=O at 536.37 eV) core levels (Fig. 2b, c) increased with respect to the contributions associated to SiOx at 107.62 and 537.23 eV, respectively) and SiC (105.62 eV). The S2p core level showed a single component at 167.22 eV [22], stemming from the C–S group in MPTMS (Fig. 2d).

The presence of Sulphur and the enhancement of chemical species that are related to MPTMS suggest that functionalization of the NWs successfully occurred. Besides this, the reduction of features specific of NWs only is the evidence of an existing overlayer coating the inorganic surface. Due to the complex structure of these nanowires, it is difficult to evaluate the organic film thickness and coverage from photoemission signal reduction and/or increase. However, considering a reasonable value of 1–2 nm for the inelastic mean free path of Si2p in the organic layer, a reasonable thickness of about 2 nm can be supposed, which is typical of a single MPTMS monolayer.

3.2 Nanowire functionalization enhances surface electronegativity

Even though XPS highlighted the presence of decorations on NWs, their wettability was measured. This assay showed a change between bare and treated NWs, confirming the presence of decorating molecules on the NW surface. As expected, MPTMS functionalization increased the electronegativity of the NWs compared to control NWs (Fig. 3).

3.3 Functionalization alters protein adsorption profile on NWs

The effect of MPTMS decoration on the adsorption of serum proteins to NWs was investigated by SDS-PAGE. The representative experiment reported in Fig. 4 shows that MPTMS functionalization not only reduced the total amount of adsorbed serum proteins by the NWs, but also changed the pattern of NWs interacting with the proteins. In particular, while the bulk of adsorbed proteins corresponded to albumin region for both NWs and MPTMS-NWs, MPTMS modification led to the complete disappearance of a group of proteins with a MW between 100 and 130 kDa that were, instead, clearly adsorbed by pristine NWs (Fig. 4, NWS lane, middle arrow). In addition, surface modification strongly reduced the amount of adsorbed proteins with a MW around 25 kDa (Fig. 4, NWS lane, bottom arrow), whereas promoted the adsorption of a group of proteins with a MW around 180 kDa, which were detectable in total serum proteins but not in protein samples eluted from pristine NWs (Fig. 4, NWS lane, upmost arrow).

	NWs	MPTMS-NWs
Z-Potential	-3,15 mV	-6,53 mV

Fig. 3 Z-Potential results

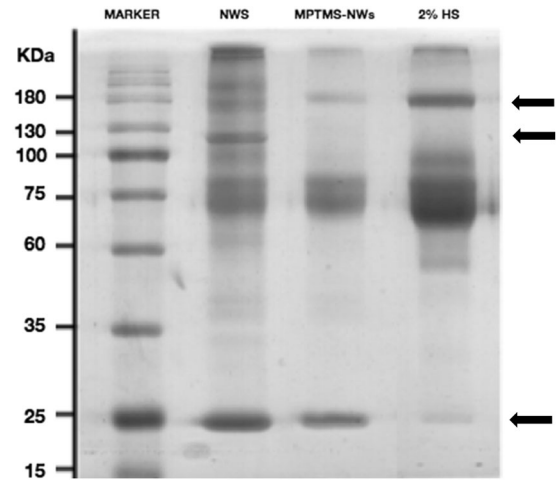

Fig. 4 SDS-PAGE and Comassie Blue staining of proteins adsorbed on native or functionalized NWs after incubation with 2% HS in PBS

3.4 Nanowire functionalization improves cell proliferation

MPTMS functionalization did not influence cell viability after 24 h of culture, when no differences were observed between the groups, however a highly significant increase of cell viability was detected in cells on MPTMS-NWs after 48 h (Fig. 5), which suggests that cells could grow more effectively in the presence of the functionalization.

Consistent with this, LIVE/DEAD assay results indicated that cells were numerous on the MPTMS-NWs after 48 h, than on control NWs (Fig. S1–Sn).

3.5 Nanowire functionalization affects cell morphology

Since adsorbed proteins may affect cell adhesion on substrates [23], we proceeded to investigate the morphology of murine pre-osteoblastic calvaria cells on control and MPTMS-NWs by SEM analysis (Fig. 6).

After 48 h of culture, cells appeared well-spread on samples from both groups, with the typical polygonal morphology [24]. Cells on MPTMS-NWs appeared larger and with several cytoplasmic extroflections to grant the cell body an adequate anchorage to the material (Fig. 6d). NWs in both groups appeared able to cross the cell cytoplasm, which was often observed surrounding the silicon oxycarbide structures and sometimes pierced by them (Fig. 6b, e). Moreover, FIB analysis revealed that cells were not able to grow into the NWs meshwork, as the gaps between individual nanowires were not large enough to allow cells to

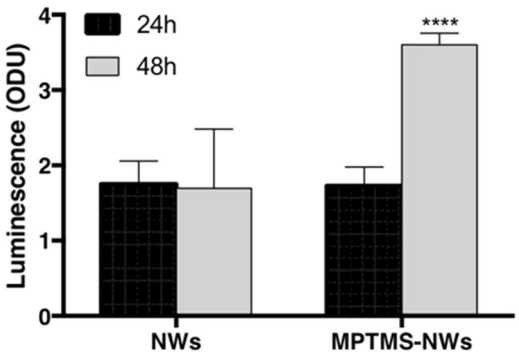

Fig. 5 Chemiluminescence-based cell viability assay of MC3T3-E1 cells on control or MPTMS-NWs after 24 or 48 h of culture. **** $p <$ 0.0001

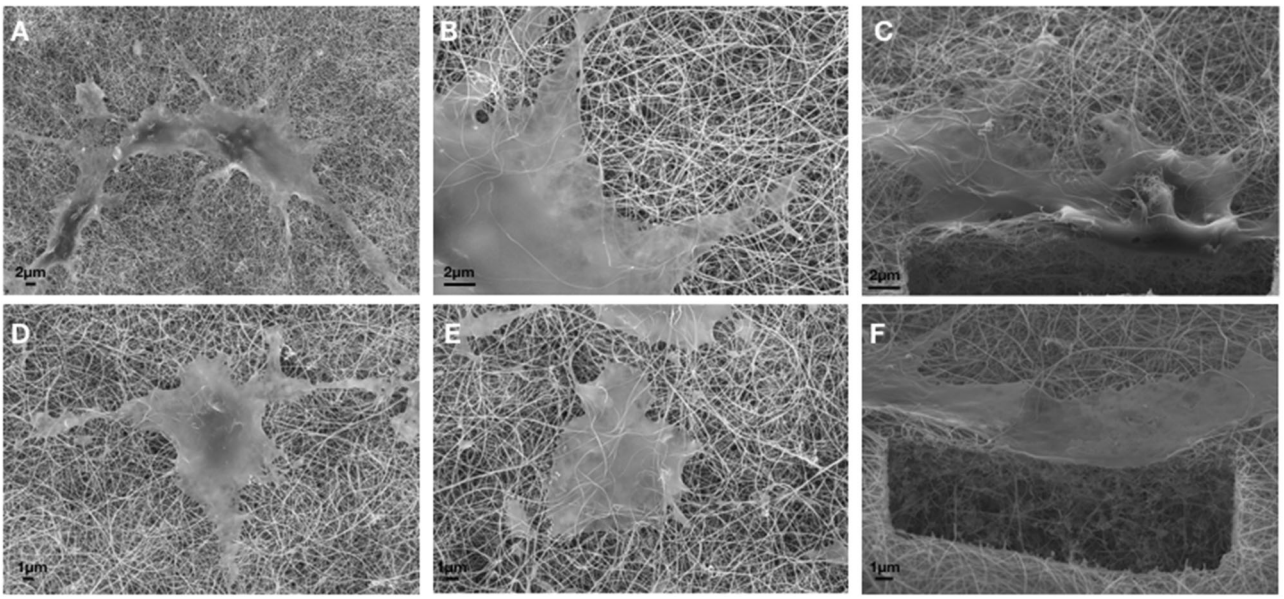

Fig. 6 SEM images of MC3T3-E1 cells on control **a**–**c** or functionalized NWs **d**–**f** after 48 h of culture. Cells were sectioned by FIB **c**, **f**, revealing the underlying structure

creep in but remained anchored to the superficial layer of nanowires (Fig. 6c, f).

3.6 Nanowire functionalization improves focal adhesion

To investigate whether MPTMS-NWs provided a better substrate for cell attachment and to support SEM-FIB observation, MC3T3-E1 cells were labelled with vinculin, a protein which participates in constituting focal adhesions, multi-molecular complexes involved in attaching cells to their substrate [25]. Cells were also marked for actin cytoskeleton through TRITC-phalloidin and for nuclei through DAPI. Consistent with SEM observations, cells on MPTMS-NWs appeared larger and with more numerous small extroflections (Fig. 7b) supported by a visible, robust cytoskeleton apparatus (Fig. 7d–f), possibly filopodia. Vinculin appeared as discrete dot-like labels in control NWs (Fig. 7e), indicating that cell-substrate contact points were mostly small and discrete, consistently with the narrow profile of the nanowires. However, in the presence of functionalized NWs, vinculin marking appeared more diffused throughout the cytoplasm, suggesting that cells were able to establish wider and more numerous anchorage points, confirming the results obtained with SEM-FIB observation (Fig. 7d). Large actin stress fibers running through the cell body were also visible in cells on functionalized NWs, but were remarkably absent from cells cultured on control NWs, indicating that NW decoration could improve cell adhesion (Fig. 7d).

3.7 Nanowire functionalization ameliorates gene expression profile in osteoblasts

After morphological and viability analysis, we moved on to assaying gene expression in MC3T3 cells on NWs (Fig. 8).

A scaffold material for tissue regeneration should support the expression of an array of genes that are conductive to achieve an adequate cell phenotype to tissue deposition. For this reason, we were mostly interested in osteoblast-specific genes, such as Alkaline Phosphatase, or in matrix associated genes, which would indicate that cells are prompted to become osteoblasts and deposit new matrix material. Interestingly, significantly higher levels of transcript for the early osteoblastic markers Alkaline Phosphatase (ALP) and Collagen I (COL1A1) were detected in cells grown on MPTMS-NWs. No differences were, however, observed in the levels of the mature marker osteocalcin (OCN) and in the osteoblast-specific transcription factor Runx2. This result is promising, as the expression of higher levels of early stage osteoblastic markers supports the idea that this substrate can provide a microenvironment capable to promote a commitment down the osteoblastic lineage, although by 96 h cells did not reach a mature phenotype yet. The expression of matrix main component collagen I was also increased on MPTMS-NWs.

4 Discussion

As novel biomaterials are being designed and tested, the spectrum of possibilities for regenerative therapies

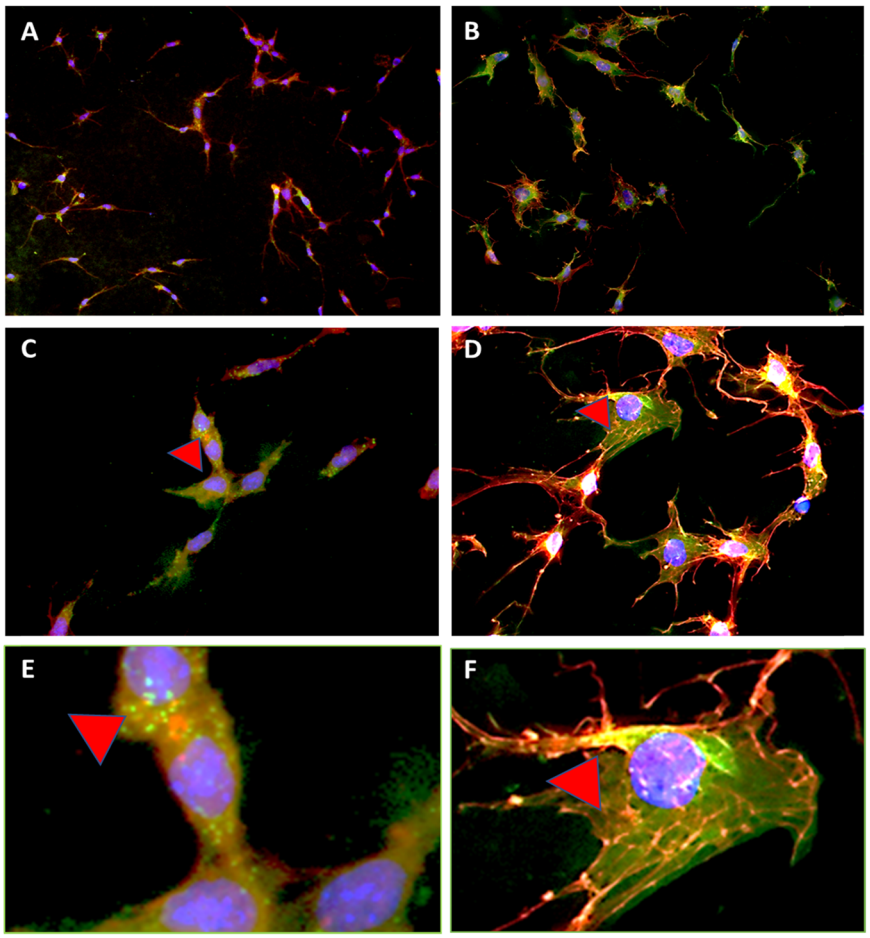

Fig. 7 Immunofluorescence labeling of vinculin (green), actin (red) and nuclei (blue) in MC3T3-E1 cells cultured on control NWs **a**, **c**, **e** or functionalized NWs **b**, **d**, **f** after 48 h of culture. Red arrows underline the morphology of focal adhesion. Magnification: **a**, **b** 20×, **c**, **d** 40×, **e**, **f** details of image **c**, **d**, respectively

broadens. The introduction of nano-patterned materials and nanodimensional materials has opened the potential to effectively create materials that can mimic the nanofeatures of natural tissues [26]. The extracellular matrix (ECM), the main component of connective tissue, is a complex of collagen and non-collageneous proteins arranged in a 3D meshwork. This network hosts and supports cells and regulates their function by offering adhesion sites and a vast array of biochemical and physical cues that trigger or suppress cell differentiation and activity [27]. Far from being a bulk material, ECM is made of filamentous molecules, e.g., collagen and proteoglycans, whose fibrils and fibers are interspersed with water that allows for cell communication [28]. Nanowires (NWs) strongly resemble this morphology and the idea that NWs could be used to recreate this 3D organization as an implantable scaffold is fascinating. We recently published the results of a study investigating the biocompatibility of SiO_xC_y NWs with murine fibroblastic cells and have outlined the possibility to used them as scaffolds [13]. A scaffold, however, should not only be biocompatible, but it should also promote cell attachment and adhesion and support the physiological assembly of protein species on its surface [29], for the sake of improved biomimetics [30]. We therefore turned to exploring whether decorating these NWs with reactive functional groups could confer them with a higher capability to bind proteins and cells. To this purpose we used 3-mercaptopropyltrimethoxysilane (MPTMS), a compound that possesses a free –SH group available to bind other thiol groups, e.g., in the lateral chains of plasma proteins, to functionalize the surface of the NW and possibly ending up by masquerading the exogenous biomaterial under a layer of firmly adsorbed proteins. As far as the adsorption of serum proteins is concerned, it is quite evident that MPTMS modification completely changes the interaction of NWs with selected serum protein. In particular, surface modified NWs are overall less adsorbent than pristine ones but, at the same time, they are more selective for a specific group of proteins present in human serum. Indeed, as shown in Fig. 4, MPTMS-NWs efficiently adsorb proteins around 180 kDa, a molecular weight matching that of fibronectin. Interestingly, this property was not shared by pristine NWs. Although, the adsorbed serum proteins were not identified in this contribution, the preferential adsorption of fibronectin by MPTMS-NWs is not only consistent with data on cell spreading but could represent a mechanism underlying

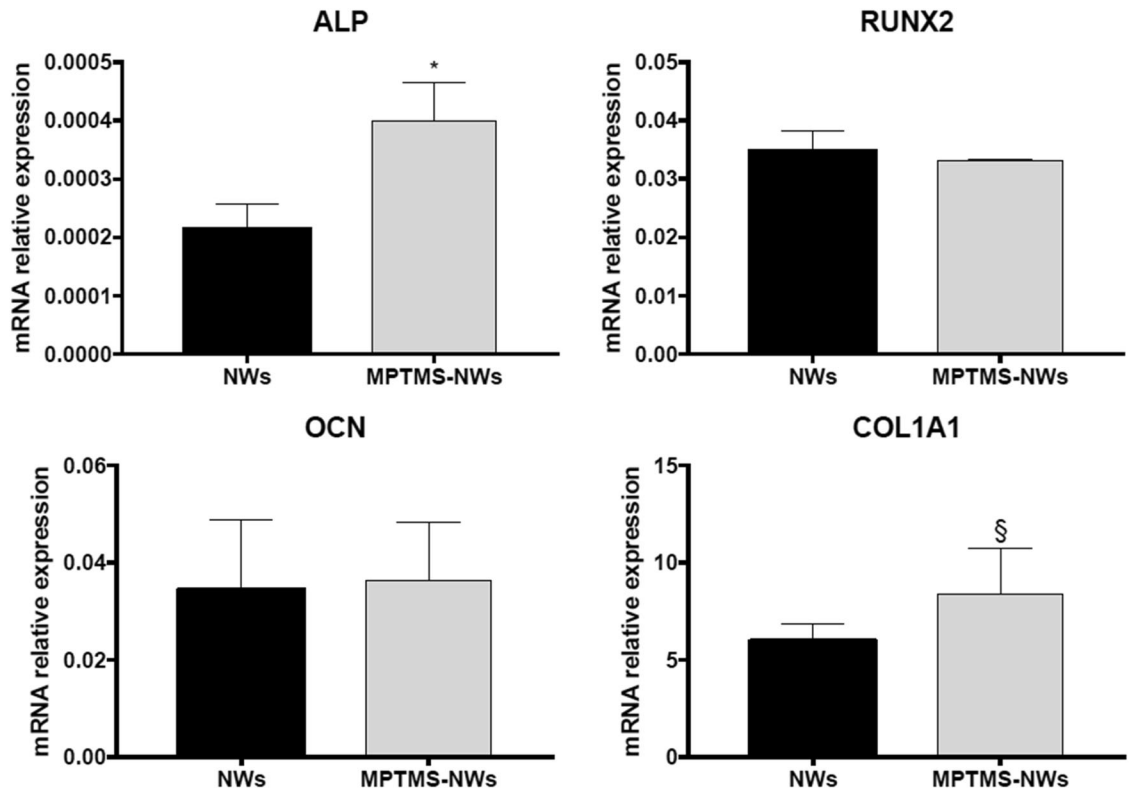

Fig. 8 Quantitative RT-PCR of alkaline phosphatase **a**, Runx2 **b**, Osteocalcin **c** and Collagen I **d** mRNA from MC3T3-E1 cells cultured on control or MPTMS-NWs. All values were normalized to GAPDH mRNA levels. Values are reported as mean ± standard deviation. $^{*}P = 0.02$; $^{\S}P = 0.04$

the effects of surface modification on osteoblastic differentiation.

We then tested cell responses to these modified NWs and we chose MC3T3 cells because they are an established model of murine osteoblasts [29]. As bone is a tissue where grafting is a common routine practice and the need for more effective implant materials is relevant, we opted for a cell model that more closely resembled a possible final application than just L929 cells [31, 32].

When cells were seeded on control or decorated NWs, it became apparent that MPTMS functionalization could be a promising solution to overcome the problems with cell growth we previously encountered on NWs [13]. In our previous paper, L929 cells attached to nanowires but did not show remarkable cell growth on SiO_xC_y NWs. Cell numbers remained essentially stationary over the culture period. On the contrary, MC3T3 osteoblastic cells appear to grow more rapidly on MPTMS-SiO_xC_y NWs, which is a promising result for scaffold colonization.

Importantly, cell morphology was positively affected by MPTMS functionalization and cells possessed a larger cell body. This is highly indicative of improved adhesion as cells can flatten out on a surface only after they have firmly adhered to it, so that their cytoskeleton can start to contract and the cell body spreads out and becomes thinner and larger. Cell adhesion is an important process in the normal progression of the cell cycle. Its process is at the base of the control of cell growth, differentiation during development and spreading behavior [33]. Cell attachment and spreading on biomaterials are mediated by a highly complex structure called focal adhesion which is a multi-protein, microscale assembly involving the clustering of ligated transmembrane receptor integrins at the nanoscale [34]. It has been shown that the spacing between the integrin ligands is important to integrin clustering and focal adhesion. There is more evidence that clustering of integrins to assembly requires a spacing between ligated integrins of around 50–70 nm [35]. Nanotopographies with spacings >100 nm may actually inhibit cell adhesion by opposing a correct clustering of integrins into focal adhesions [36]. As single NW offers a limited space for focal adhesions and are separated by large gaps, on a cellular scale, which may actually be restraining the formation of focal adhesion.

This is corroborated by the immunofluorescence microphotographs that show large, red-stained actin fibers crossing the cytoplasm of cells on decorated NWs. These large actin bundles are known as stress fibers and are typically arranged along the force vectors that are generated by actomyosin complexes within the fibers. Stress fibers only form after solid focal adhesion have formed and

possibly cluster [37]. Interestingly, no such stress fibers are visible on control NWs indeed the focal adhesion appears dot shape, possibly because their diameter is around 100 nm and the gap between nanowires ranges from hundred nm to several microns. Hence, although integrin clustering may occur on a single nanowire, the microscale focal adhesion assembly can be impaired because of the long distances between nanowires. NW functionalization may provide a more favorable protein microenvironment to promote the formation of solid focal adhesion and FA clusters and, therefore, improved cell adhesion.

The NW meshwork, as it is now, does not yet allow for cell in-growth, as gaps between single NWs are still too small for cell bodies to creep in between. This arrangement may have to be modified by tuning the amount and density of NWs for proper colonization. However, we have already shown that L929 cells are capable to mold the NW scaffold and modify it to adjust it to their topographical needs [11]. We then investigated cell differentiation by measuring the expression of specific ECM and osteoblastic genes. Care must be taken when assessing cell differentiation in cell lines, as this process has been modified from what can be observed in primary cells. However, Alkaline Phosphatase is considered a good marker of osteoblastic phenotype, which gets expressed quite early on in the process [38]. Interestingly, both ALP and Collagen I expression were upregulated on functionalized NWs. We did not observe any increase in Runx2 expression or late osteoblastic marker Osteocalcin (which is actually a target gene of Runx2) and, therefore, these decorated NWs cannot be proven to promote the expression of a late mature osteoblastic phenotype. However, this again could have positive effects on the terminal outcome of tissue integration. The first phases of scaffold colonization by primary tissue cells require cells to proliferate and, while colonizing the scaffold, differentiate to matrix-depositing mature osteoblasts. As osteoblastic differentiation is associated to a loss of proliferative capability, it can be hypothesized that, if cells matured too quickly, this might compromise the colonization of the scaffold. Future studies will have to investigate this issue more thoroughly.

5 Conclusion

Three-mercaptopropyltrimethoxysilane functionalization of silicon oxycarbide nanowires appears as a viable strategy to improve the compatibility of these nanostructures. Firstly, the presence of the functionalization leads to a change in the adsorbed protein pattern; cellular response to the biomaterial in terms of cell proliferation was enhanced on MPTMS-NWs compared to bare NW controls. SEM-FIB observation showed healthy cells with polygonal shape on both NWs. Focal adhesion staining displayed a higher amount of vinculin in the cytoplasm of cells grown on MPTMS-NWs, verifying the better adhesion of cells to the functionalized material. We have shown that focal adhesions on control samples were fewer and more isolated, while on MPTMS-NWs they were homogeneously distributed in the cytoplasm. RT-PCR results showed an enhancement of mRNA expression of the principal marker of early osteoblastic commitment (ALP) on MPTMS-NWs, confirming the induction of cells through osteoblastic differentiation. Taken together, these data suggest that MPTMS functionalization enhances the response of bone cells to the substrate, promoting their proliferation, as well as the expression of osteoblastic markers, making MPTMS-NWs a promising scaffold coating for biomedical applications.

Acknowledgements The authors would like to thank Dr. Galli Gianfranco (Dip. Scienze Matematiche, Fisiche e Informatiche, University of Parma, Parco Area delle Scienze 7/A, 43123 Parma, Italy) for his technical help in Z-potential measurements.

Author contributions The paper was written through contributions of all authors. All authors have given approval to the final version of the paper.

Compliance with ethical standards

Conflict of interest The authors declare that they have no conflict of interest.

References

1. Westcott SL, Oldenburg SJ, Lee TR, Halas NJ. Formation and adsorption of clusters of gold nanoparticles onto functionalized silica nanoparticle Surfaces. Langmuir. 1998;14:5396–401. https://doi.org/10.1021/la980380q.
2. Galli C, Parisi L, Smerieri MA, Passeri G, Guizzardi S, Costa F, et al. Improved scaffold biocompatibility through anti-fibronectin aptamer functionalization. Acta Biomater. 2016;42:147–56.
3. Bracaglia LG, Smith BT, Watson E, Arumugasaamy N, Mikos AG, Fisher JP. 3D printing for the design and fabrication of polymer-based gradient scaffolds. Acta Biomater. 2017;56:3–13.
4. Lumetti S, Consolo U, Galli C, Multinu A, Piersanti L, Bellini P5, et al. Fresh-frozen bone blocks for horizontal ridge augmentation in the upper maxilla: 6-month outcomes of a randomized controlled trial.Clin Implant Dent Relat Res. 2014;16:116–23.
5. Mebarki M, Coquelin L, Layrolle P, Battaglia S, Tossou M, Hernigou P, et al. Enhanced human bone marrow mesenchymal stromal cell adhesion on scaffolds promotes cell survival and bone formation. Acta Biomater. 2017;59:94–107.
6. Ghiacci G, Graiani G, Ravanetti F, Lumetti S, Manfredi E, Galli C, et al. Over-inlay' block graft and differential morphometry: a novel block graft model to study bone regeneration and host-to-graft interfaces in rats. J Periodontal Implant Sci. 2016;46:220–33.
7. Galli C, Parisi L, Elviri L, Bianchera A, Smerieri A, Lagonegro P, et al. Chitosan scaffold modified with D-(+) raffinose and

enriched with thiol-modified gelatin for improved osteoblast adhesion. Biomed Mater. 2016;11:015004
8. Parisi L, Galli C, Bianchera A, Lagonegro P, Elviri L, Smerieri A, et al. Anti-fibronectin aptamers improve the colonization of chitosan films modified with D-(+) Raffinose by murine osteoblastic cells. J Mater Sci Mater Med. 2017;28:136
9. Anselme K, Davidson P, Popa AM, Giazzon M, Liley M, Ploux L. The interaction of cells and bacteria with surfaces structured at the nanometre scale. Acta Biomater. 2010;6:3824–46.
10. An J, Chua CK, Yu T, Li H, Tan LP. Advanced nanobiomaterial strategies for the development of organized tissue engineering constructs. Nanomed (Lond). 2013;8:591–602.
11. Mark KV on Der, Park J, Bauer S, Schmuki P. Nanoscale engineering of biomimetic surfaces: cues from the extracellular matrix. Cell Tissue Res. 2010;339:131–53.
12. Kuo S-W, Lin HI, Ho JH, Shih YR, Chen HF, Yen TJ, et al. Regulation of the fate of human mesenchymal stem cells by mechanical and stereo-topographical cues provided by silicon nanowires. Biomaterials. 2012;33:5013–22.
13. Lagonegro P, Rossi F, Galli C, Smerieri A, Alinovi R, Pinelli S, et al. A cytotoxicity study of silicon oxycarbide nanowires as cell scaffold for biomedical applications. Mater Sci Eng C. 2017;73:465–71.
14. Tamayo A, Rubio J, Rubio F, Oteo JL, Riedel R. Texture and micro-nanostructure of porous silicon oxycarbide glasses prepared from hybrid materials aged in different solvents. J Eur Ceram Soc. 2011;31:1791–801.
15. Gourevitch D, Kossenkov AV, Zhang Y, Clark L, Chang C, Showe LC, et al. Inflammation and its correlates in regenerative wound healing: an alternate. Perspect, Adv Wound care. 2014;3:592–603.
16. Fabbri F, Rossi F, Melucci M, Manet I, Attolini G, Favaretto L, et al. Optical properties of hybrid T3Pyr/SiO2/3C-SiC nanowires. Nanoscale Res Lett. 2012;7:680
17. Rossi F, Bedogni E, Bigi F, Rimoldi T, Cristofolini L, Pinelli S, et al. Porphyrin conjugated SiC/SiOx nanowires for X-ray-excited photodynamic therapy. Sci Rep. 2015;5:7606
18. Curran JM, Chen R, Hunt JA. The guidance of human mesenchymal stem cell differentiation in vitro by controlled modifications to the cell substrate. Biomaterials. 2006;27:4783–93.
19. Negri M, Dhanabalan SC, Attolini G, Lagonegro P, Campanini M, Bosi M, et al. Tuning the radial structure of core-shell silicon carbide nanowires. CrystEngComm. 2015;17:1258–63.
20. Fabbri F, Rossi F, Negri M, Tatti R, Aversa L, Dhanabalan SC, et al. Carbon-doped SiO(x) nanowires with a large yield of white emission. Nanotechnology. 2014;25:185704
21. Chastain J, Moulder JF, King RC, et al. Handbook of X-ray photoelectron spectroscopy: a reference book of standard spectra for identification and interpretation of XPS data. Physical electronics, Eden Prairie, Minn.: [s.n.], 1992.
22. Tatti R, Timpel M, Nardi MV, Fabbri F, Rossi R, Pasquardini L, et al. Surface functionalization of nanowires by supersonic molecular beams: demonstration of a hybrid SiC/SiO2/H2TPP(F) nanosystem for X-Ray induced singlet oxygen generation. Mol Syst Des Eng. 2017;2:165
23. Sun M, Deng J, Gao C. The correlation between fibronectin adsorption and attachment of vascular cells on heparinized polycaprolactone membrane. J Colloid Interface Sci. 2015;448:231–7.
24. Galli C, Piemontese M, Lumetti S, Ravanetti F, MacAluso GM, Passeri G. Actin cytoskeleton controls activation of Wnt/β-catenin signaling in mesenchymal cells on implant surfaces with different topographies. Acta Biomater. 2012;8:2963–8.
25. Bays JL, DeMali KA. Vinculin in cell–cell and cell–matrix adhesions. Cell Mol Life Sci. 2017;74:2999–3009.
26. Zhang L, Webster TJ. Nanotechnology and nanomaterials: promises for improved tissue regeneration. Nano Today. 2009;4:66–80.
27. Mackiewicz Z, Konttinen YT, Kaivosoja E, Stegajev V, Wagner HD, Levón J, et al. Extracellular matrix and tissue regeneration. In: Steinhoff G (Ed.). Regenerative Medicine—from Protocol to Patient. Cham: Springer International Publishing; 2016. p. 1–55.
28. Frantz C, Stewart KM, Weaver VM. The extracellular matrix at a glance. J Cell Sci. 2010;123(Pt 24):4195–200.
29. Wilson CJ, Clegg RE, Leavesley DI, Pearcy MJ. Mediation of biomaterial–cell interactions by adsorbed proteins: a review. Tissue Eng. 2005;11:1–18.
30. Choi J, Hwang J, Jeong Y, Park JM, Lee KH, Hong JW. Biomimetics: forecasting the future of science, engineering, and medicine. Int J Nanomed. 2015;10:5701.
31. Sudo H, Kodama HA, Amagai Y, Yamamoto S, Kasai S. In vitro differentiation and calcification in a new clonal osteogenic cell line derived from newborn mouse calvaria. J Cell Biol. 1983;96:191–8.
32. Wang D, Christensen K, Chawla K, Xiao G, Krebsbach PH, Franceschi RT. Isolation and characterization of MC3T3-E1 preosteoblast subclones with distinct in vitro and in vivo differentiation/mineralization potential. J Bone Miner Res. 1999;14:893–903.
33. Hayashi Y, Furue MK, Okamoto T, Ohnuma K, Myoishi Y, Fukuhara Y, et al. Integrins regulate mouse embryonic stem cell self-renewal. Stem Cells. 2007;25:3005–15.
34. Bershadsky A, Kozlov M, Geiger B. Adhesion-mediated mechanosensitivity: a time to experiment, and a time to theorize introduction: why are cell adhesions mechanosensitive? Curr Opin Cell Biol. 2006;18:472–81.
35. Cavalcanti-Adam EA, Micoulet A, Blümmel J, Auernheimer J, Kessler H, Spatz JP. Lateral spacing of integrin ligands influences cell spreading and focal adhesion assembly. Eur J Cell Biol. 2006;85:219–24. Epub 2005 Oct 10.
36. Yim EKF, Darling EM, Kulangara K, Guilak F, Leong KW. Nanotopography-induced changes in focal adhesions, cytoskeletal organization, and mechanical properties of human mesenchymal stem cells. Biomaterials. 2010;31:1299–306.
37. Tojkander S, Gateva G, Lappalainen P. Actin stress fibers - assembly, dynamics and biological roles. J Cell Sci. 2012;125:1855–64.
38. Farley JR, Hall SL, Tanner MA, Wergedal JE. Specific activity of skeletal alkaline phosphatase in human osteoblast-line cells regulated by phosphate, phosphate esters, and phosphate analogs and release of alkaline phosphatase activity inversely regulated by calcium. J Bone Miner Res. 1994;9:497–508.